

Structural Characterization of Tungsten Oxides Supported on Titanium Silicalite

Didik Prasetyoko¹, Zainab Ramli², Salasiah Endud² and Hadi Nur³

Abstract—Titanium silicalite (TS-1) is known as an active material catalyst in the epoxidation reaction. In this study, tungsten oxides (WO₃) with various loading amount have been supported on the TS-1 to increase of the catalytic activity of the TS-1 material. The solids structure and property were investigated by X-ray diffraction (XRD), temperature programmed reduction (TPR), ultra violet-visible diffuse reflectance (UV-Vis-DR) and infrared (IR) spectroscopy and scanning electron microscopy (SEM) techniques. The results showed that the structure of TS-1 is not collapsed after impregnation of WO₃. It was also found that tungsten species have interacted with the silanol groups on the surface of TS-1.

Keywords—Material catalysts, titanium silicalite, tungsten oxides, characterization

I. INTRODUCTION

Since Enichem has discovered the titanosilicate-1 [1], many research groups have explored the structure, property and catalytic activity of the titanium-containing materials. It was due to the excellent activity and selectivity of TS-1 as catalysts in the various reactions such as amoxidation, hydroxylation, and oxidation [1], [2], [3]. In the epoxidation reaction, the interaction between titanium and oxidizing agents to form titanium-oxo species is well known as the key step in the determination of the rate of reaction [4]. The development of the Ti-containing molecular-sieves catalysts in order to increase its catalytic activity towards epoxides is still in progress. Fierro and co-workers have reported the effect of alkali addition to the TS-1 catalyst. They observed that the selectivity of epoxide increased as the ratio of Lewis to Brønsted acid sites increased. We have reported the catalytic performance of modified TS-1 by impregnation of niobium oxide hydrated and sulfated zirconia [5]. It was proposed that the rate of the formation of epoxide was observed to increase in the modified TS-1 catalysts containing Brønsted acid sites, due to faster formation of reactive titanium-oxo intermediate.

Tungsten oxide-zirconia catalysts with loading amount higher than monolayer capacity showed both Brønsted and Lewis acid sites [6], [7], [8]. The high acid strength and high acidity were responsible for the W=O bond

nature of complex formed by the interaction between WO₃ and ZrO₂ [9]. Generally, the structures and properties of supported metal oxide materials are strongly influenced by the metal oxide precursor, the loading amount of the metal oxide, the nature of support, and the experimental conditions. In this paper, catalysts WO₃/TS-1 were prepared by impregnation of WO₃ on the TS-1. The interaction of TS-1 and tungsten in the catalyst were examined by XRD, TPR, UV-Vis-DR, IR and SEM techniques.

II. EXPERIMENTAL

A. Sample Preparation

The support, titanium silicalite (TS-1, 3 mol% titanium) was prepared according to a procedure described earlier [1]. The WO_x/TS-1 catalysts were prepared by incipient wetness impregnation of TS-1 with an aqueous solution containing sufficient amount of ammonium metatungstate hydrate (NH₄)₆ H₂W₁₂O₄₁ · 18H₂O, to yield materials with loading in the ranges of 2–25 wt% of WO₃ in the calcined state. The suspension was heated at 110°C for 3 h under stirring condition, followed by evaporation of water, drying at 110°C for 24 h, and calcination at 550°C for 6 h. The samples denoted by their weight percentage of WO₃ on TS-1 (Table 1).

TABLE I
AMOUNT OF WO₃ LOADING OF THE SAMPLES USING NEUTRAL PREPARATION CONDITIONS

Sample	WO ₃ , wt%
TS-1	0
2WO ₃ /TS-1	2.4
5WO ₃ /TS-1	4.9
7WO ₃ /TS-1	7.2
10WO ₃ /TS-1	9.7
15WO ₃ /TS-1	14.6
25WO ₃ /TS-1	24.9

B. Characterization

The samples were characterized by powder X-ray diffraction (XRD) for the crystallinity and phase content of the solid materials using a Bruker Advance D8 Diffractometer with the Cu Kα (λ=1.5405 Å) radiation as the diffracted monochromatic beam at 40 kV and 40 mA. The pattern was scanned in the 2θ ranges from 5° to 50° at a step size 0.010° and step time 1s. The reducibility of the surface species was determined by temperature-programmed reduction (TPR) of the samples using a TPDRO 1100 Thermofinnigan apparatus equipped with a thermal

Manuscript received March 7, 2007; revised September 30, 2007

¹ Didik Prasetyoko is with department of chemistry, FMIPA, Institut Teknologi Sepuluh Nopember, Surabaya, INDONESIA (email: dramadhani@yahoo.com)

² Zainab Ramli and Salasiah Endud are with department of chemistry, faculty of science, universiti teknologi malaysia, 81310 utm skudai, johor, MALAYSIA

³ Hadi Nur is with Ibnu Sina Institute for fundamental science studies, universiti teknologi malaysia, 81310 utm skudai, johor, MALAYSIA

conductivity detector. The samples were calcined in static air at 550°C for 6 h before loaded in the quartz tube. The samples were pretreated in the stream of nitrogen with flow rate 40 ml/min (99.999%) at 100°C for 2 h. The reduction was performed with hydrogen in nitrogen (50 ml/min; 5% H₂ in N₂) from 100°C to 1000°C with heating rate of 10°C and held at final temperature for 30 min. The hydroxyl groups of the samples were monitored by Fourier Transform Infrared (FTIR) spectroscopy technique. The wafer of the sample (10-12 mg) was locked in the cell equipped with CaF₂ windows, and evacuated at 400°C under vacuum condition for 4 h. Infrared spectra of the sample were recorded at room temperature in the region of 4000 – 3000 cm⁻¹ on a Shimadzu FTIR, with a spectral resolution of 2 cm⁻¹, scans 10 s, at temperature 20°C. UV-vis DR spectra were recorded under ambient conditions using a Perkin-Elmer Lambda 900 UV/VIS-NIR spectrometer. The spectra were monitored in the range of 190–600 nm. Morphology of the TS-1 samples were monitored by SEM technique. Samples were poured on the stubs with double tape. Gold coating of the sample was performed by Bio Rad SEM Coating System at 10⁻¹ mbar with 30 mA for 75 minutes. Stubs containing sample was placed inside the electron microscope model Philip XL40 under vacuum at 5 bar. SEM micrograph was recorded with resolution of 30 kV.

III. RESULT AND DISCUSSION

A. X-ray Diffraction

The XRD patterns of the TS-1 and WO₃/TS-1 samples with various tungsten loading and condition are shown in Fig. 1. The peaks corresponding to the crystalline phase of WO₃ at 2θ = 23.1, 23.7, 24.4, 33.2-34.6, and 41.5° (marks by arrow, in which the peaks at 2θ = 23-25° overlapping with the peaks of TS-1) is only observed for the WO₃/TS-1 samples with high amount of tungsten loading, *ca.* 10, 15 and 25wt%. The crystalline phase of WO₃ were not observed for the WO₃/TS-1 samples with low loading amount of WO₃, *ca.* 2, 5 and 7wt%. The result demonstrates that crystalline WO₃ appears only in samples with high loading while the WO₃ exists as highly dispersed species in the low loading samples. This finding is in a good agreement [10] in which the characteristic peaks of crystalline WO₃ were clearly seen for the samples with high loading amount of WO₃, *ca.* >6% and 10%, depending on the nature of support.

Fig. 2 shows the correlation of the surface concentration of the tungsten vs. the ratio of the diffraction peak intensity of WO₃ to that of TS-1 ($I_{\text{WO}_3}/I_{\text{TS-1}}$; 2θ: 34.17°/23.04°) in various WO₃ loading. Based on this graph, the dispersion capacity of tungsten on the titanium silicalite support was evaluated to be 0.35 W⁶⁺ cations/nm², by extrapolating the straight line to get the intercept on the abscissa. For comparison, the dispersion capacity of the WO₃ on TiO₂ anatase by using similar characterization and technique was reported to be 4.85 W⁶⁺/nm² of TiO₂ [11], which comparable with dispersion capacity of the WO₃ on ceria, *ca.* 4.8 W⁶⁺/nm² (Dong *et al.*, 2000). While on silica support, the dispersion capacity of WO₃ was 0.5 W⁶⁺/nm² [10]. On TS-1 support, the dispersion capacity

of WO₃ is much lower than that of anatase and ceria supports, and near to the silica support, in which these supports have lower surface area (below 300 m²/g). It seems to deduce that surface interaction between WO₃ with TS-1 is evidently different from that of WO₃ with anatase and ceria, but almost the same with WO₃ and silica. This might be due to the highly crystalline phase of TS-1, causes weak interaction of the support with the metal oxide, thus reducing the dispersion capacity of the supported metal oxides.

B. Temperature Programmed Reduction

The reduction behavior of supported tungsten oxide on alumina and silica depends on the amount of the metal oxide on the support and the interaction of the metal oxide with the support [10]. Fig. 3 shows the TPR profiles of bulk WO₃ and the TS-1 containing various amount of tungsten oxide loading. The TPR profile of 5 mg sample of bulk WO₃ exhibits two very high intense peaks of hydrogen consumed beginning at 600°C and centered at 805 and 865°C. These peaks can be assigned to the step-wise reduction of WO₃ to W, *i.e.* W(VI) → W(IV) → W(0) [12]. The TPR profiles of samples WO₃/TS-1 generally show similar reduction temperature, *i.e.* a broad reduction peak from around 400°C to 600°C and two high intense reduction peaks centered at around 750 and 800°C. According to reference [13], [14], the broad peak is assigned to octahedrally coordinated tungsten species. It was found that the amount of hydrogen consumed corresponding to this peak increased as the amount of WO₃ loading increased, indicating that the concentration of octahedral species in the samples is increased. On the other hand, the high intense peak at around 800°C is attributed to the W⁶⁺ → W⁰ reduction of tetrahedrally coordinated amorphous WO_x species [14]. Yori [15] have reported on WO₃/ZrO₂ system that octahedrally coordinated tungstate species requires lower reduction temperature than of tetrahedral tungstate species. In this study, the reduction temperatures at around 800°C of the samples were found to shift to higher temperatures depending on the amount of WO₃ loadings. In addition, the hydrogen consumption increased with the increasing amount of WO₃ loading. This finding suggests that the amount of tetrahedral tungsten species increases as the tungsten loading increases.

Furthermore, a small peak at around 500°C is observed on samples with WO₃ loading higher than the monolayer dispersion, *i.e.* 7WO₃/TS-1, 10WO₃/TS-1, 15WO₃/TS-1 and 25WO₃/TS-1 samples. On the basis of XPS and XRD results for WO₃/α-Al₂O₃, [16] assigned the peak at 500°C was the reduction of WO₃ crystallite on top of the monolayer. In this analysis, the dispersion capacity of WO₃ calculated based on the XRD result was found to be higher than the monolayer of WO₃.

In addition, it is obtained that the amount of hydrogen consumed increased as the amount of WO₃ in the samples increased. However, similar amount of WO₃ containing in the bulk WO₃ and sample 25WO₃/TS-1 resulted in the different amount of hydrogen consumed. Although reference [16] have shown that WO₃ in the WO₃/α-Al₂O₃ cannot be reduced in one step reduction processes, here,

it is found that the amount of hydrogen consumed in the bulk WO_3 has three times higher compared to sample $25\text{WO}_3/\text{TS-1}$. This finding indicates that there are interactions between tungstate and TS-1 support in the sample $\text{WO}_3/\text{TS-1}$.

C. UV-Vis. DR Spectroscopy

The structures of tungsten oxide on the surface of TS-1 have been characterized by UV-Vis DR spectroscopy technique. Generally, there are two types of tungsten oxides based on the geometry, i.e. octahedral (O_h) and tetrahedral (T_d) structures. In the UV-Vis DR spectra, the bands corresponding to tetrahedral and octahedral tungsten species appear in the spectral range of 220 – 375 nm. In the UV-Vis DR spectra, the charge transfer transmission $\text{O}^{2-} \rightarrow \text{W}^{6+}$ is blue-shifted from around 375 nm for the pure oxide which contains tungsten in octahedral coordination to 220 nm for the pure $\text{Na}_2\text{WO}_4 \cdot 2\text{H}_2\text{O}$ which contains tetrahedral WO_4^{2-} ions [17].

The UV-Vis DR spectra of the samples $\text{WO}_3/\text{TS-1}$ containing various amounts of tungsten loading and bulk WO_3 samples are given in Fig. 4. Sample TS-1 only shows a single band at around 210 nm characteristic of tetrahedral titanium structure. The spectrum of bulk WO_3 shows a high broad band and two shoulder bands at around 370, 265 and 220 nm, respectively. The first two bands are assigned to octahedral WO_3 crystallites and polyoxotungstate species, while the latter band is assigned to tetrahedral tungsten species [12], [18]. The results confirm that bulk WO_3 contains mostly octahedral tungsten species.

For samples $\text{WO}_3/\text{TS-1}$, all the samples show similar bands centered in the range of 215–235 nm, which according to [12] are attributed to tetrahedrally coordinated W(VI) species. In addition, the band for octahedral polyoxotungstate W(VI) species at around 265 nm is not observed. Moreover, the intensity of the band at around 220 nm increases as the loading amount of tungsten increases, in which sample $25\text{WO}_3/\text{TS-1}$ shows the highest intensity among the samples. The increasing intensity of the band at 220 nm suggests that the amount of tetrahedral tungsten is also increased.

D. Infrared Spectroscopy of Hydroxyl Groups

The infrared spectra of the TS-1 and $\text{WO}_3/\text{TS-1}$ samples were recorded in the range of hydroxyl stretching region at 4000 – 3000 cm^{-1} . The infrared spectra of all samples are shown in Fig. 5. The noise of the spectra is very high for sample with high tungsten loading, ca. >10wt% renders any other hydroxyls vibration to be detected in this region. After evacuation in vacuum at 400°C for 4 h, the parent support, TS-1 sample shows an

intense band at 3726 cm^{-1} and a broad band centered at 3505 cm^{-1} . A shoulder band also can be detected between those two bands, centered at 3680 cm^{-1} . The higher frequency intense band at 3726 cm^{-1} is characteristic for silanol hydroxyl groups. However, the frequency of this band is slightly lower with respect to the typical silanol of amorphous silica (3741 cm^{-1}) [19]. The broad band at 3505 cm^{-1} associated to hydroxyl groups with hydrogen bonding of water molecule with silanol groups [19]. The last band (3680 cm^{-1}) has been assigned by Zecchina [20] to different structure of terminal hydroxyl groups in the zeolitic pores.

After deposition of tungsten in the TS-1 sample, the hydroxyl region of the spectrum changed as can be seen in Fig. 5. The band position of TS-1 sample at 3726 cm^{-1} does not shift to lower or higher frequency. However, this band becomes slightly broader with lower intensity compare to the TS-1 sample, were observed for the lower WO_3 loading, as in the $2\text{WO}_3/\text{TS-1}$, $5\text{WO}_3/\text{TS-1}$ and $7\text{WO}_3/\text{TS-1}$ samples. Similar phenomenon also appeared for a broad band at around 3505 cm^{-1} , although only observed for $2\text{WO}_3/\text{TS-1}$ and $5\text{WO}_3/\text{TS-1}$ samples. For samples with high WO_3 loading, as in the $10\text{WO}_3/\text{TS-1}$, $15\text{WO}_3/\text{TS-1}$ and $25\text{WO}_3/\text{TS-1}$ samples, the isolated silanol peak is not displayed, while the peak for hydroxyl groups with hydrogen bonding started to disappear for $7\text{WO}_3/\text{TS-1}$ sample. These observation shows that both of the hydroxyl groups of TS-1 (hydroxyl silanol and hydroxyl hydrogen bonding) are involved in the reaction with tungsten, in which the hydroxyl groups with hydrogen bonding is more reactive than that of silanol groups. In the previous study, Wang [10] found that only silanol groups involved in the reaction with tungsten.

E. Scanning Electron Microscope

Samples morphology were monitored using electron microscope. Fig. 6 shows the SEM images of TS-1 and $\text{WO}_3/\text{TS-1}$ materials. The SEM image shows that TS-1 has two morphology, i.e. single and twinned crystal shape. The crystal size around 0.2-0.8 x 0.5-1 x 1-2.5, in which twinned shape has larger crystals size than single shape. The morphology of TS-1 is not affected by impregnation of 5 wt% tungsten oxide on the surface of TS-1. Similar with the XRD technique, SEM cannot monitor the evident of tungsten oxide in the sample $5\text{WO}_3/\text{TS-1}$. This finding indicated the high dispersion of tungsten on the surface of TS-1. Meanwhile, a grubby TS-1 crystal is observed in the sample $25\text{WO}_3/\text{TS-1}$. Based on the XRD finding, this sample contained tungsten oxide crystal. Therefore, it is concluded that a small particle observed on the surface of TS-1 is tungsten oxide. However, the morphology of TS-1 is not affected by impregnation of tungsten oxides.

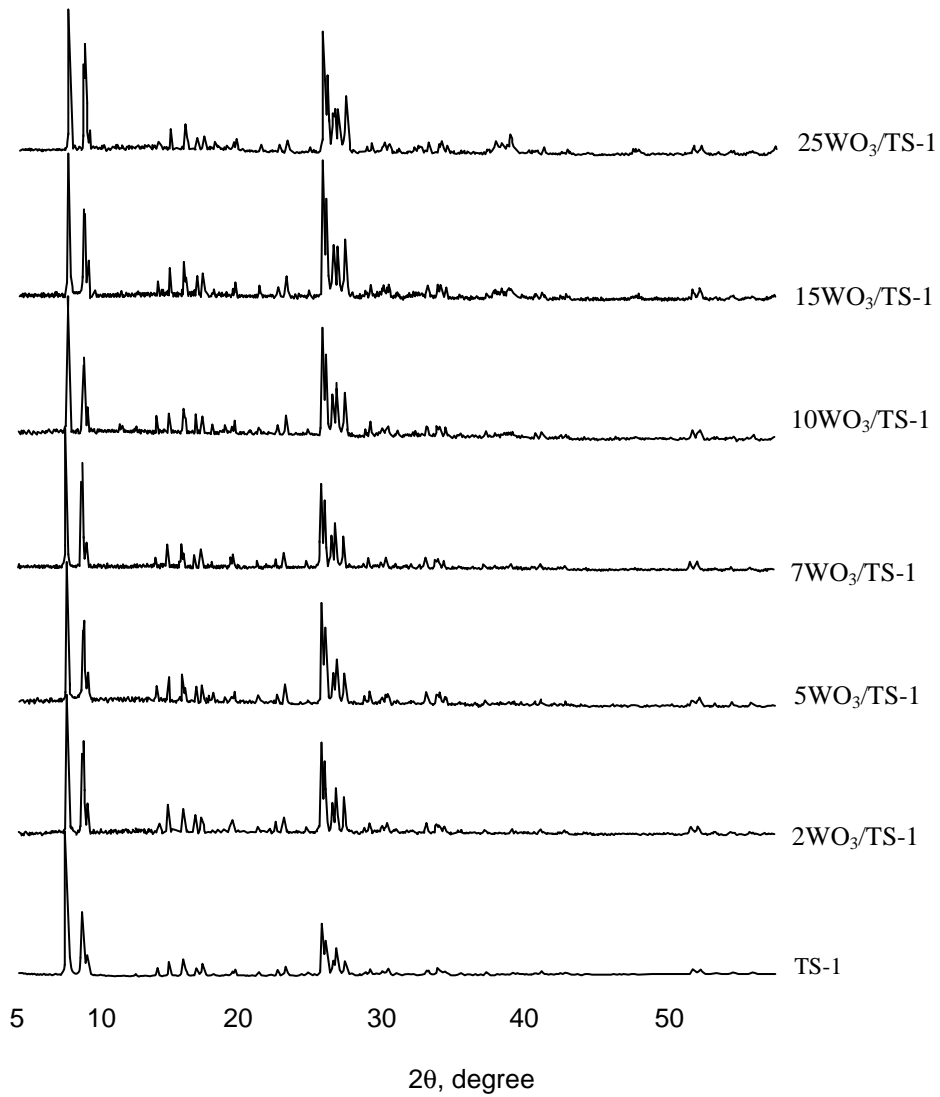


Fig. 1: XRD patterns of the TS-1 and tungsten-coated TS-1 samples

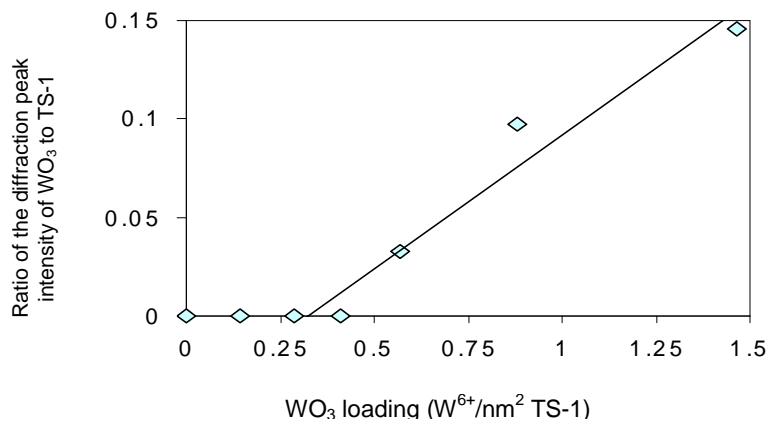


Fig. 2: The WO₃ content vs. XRD peak intensity ratio of WO₃ to TS-1 in the samples

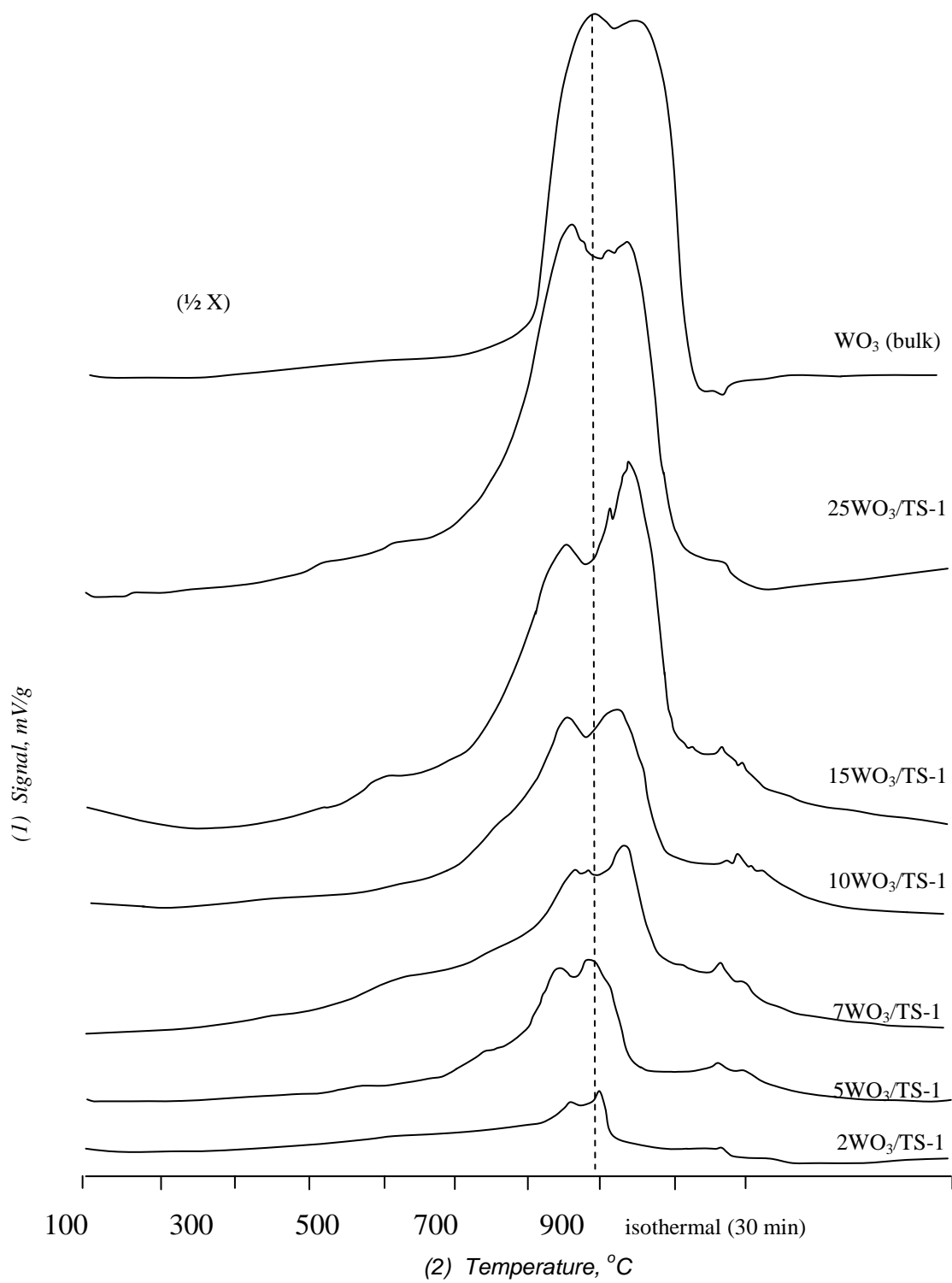


Fig. 3. TPR profiles of bulk WO₃ and WO₃/TS-1 samples

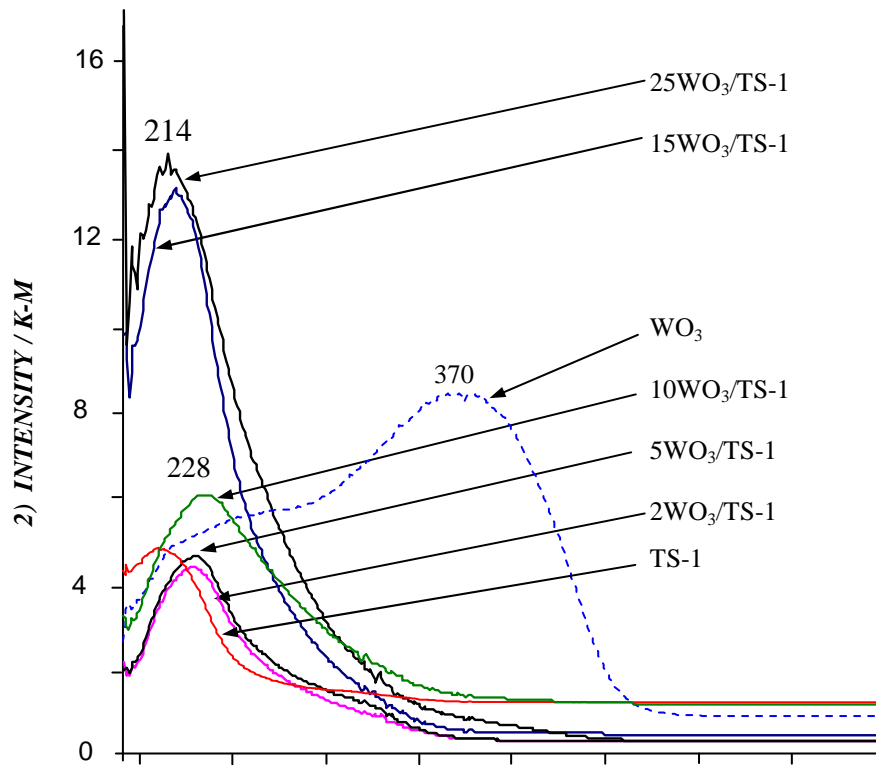


Fig. 4. UV-Visible DR spectra of TS-1, WO_3 , and $\text{WO}_3/\text{TS-1}$ samples.

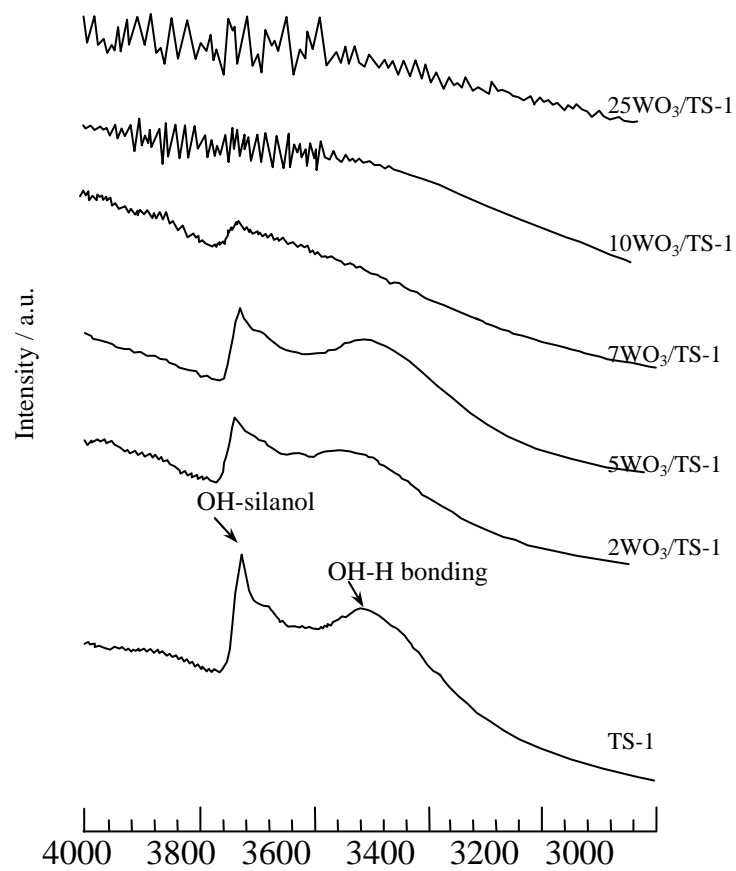


Fig. 5. Infrared spectra in the range of hydroxyl groups observation for titanium silicalite samples with different WO_3 content.

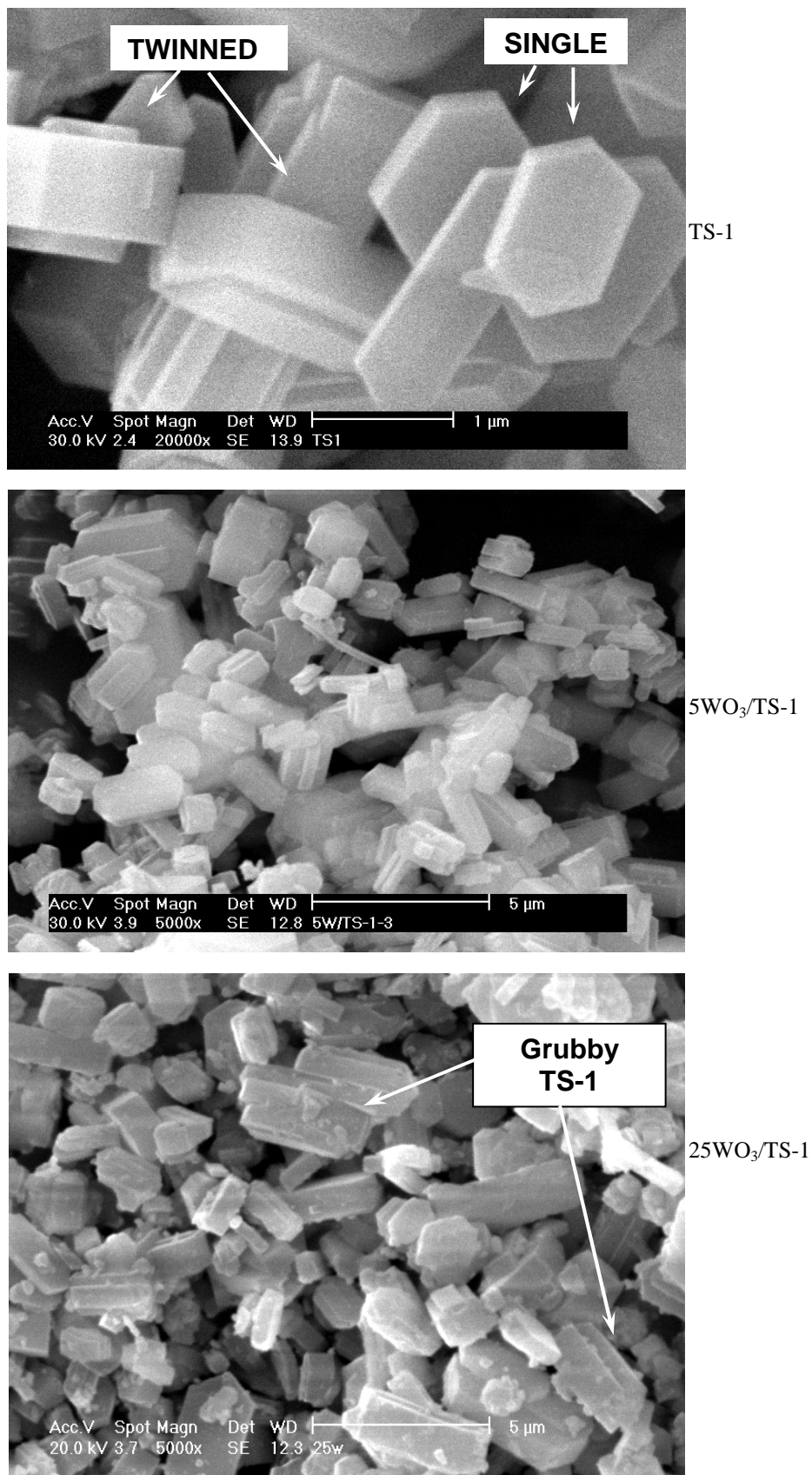


Fig. 6. The SEM images of the TS-1 materials

IV. CONCLUSIONS

The crystal structure and morphology of TS-1 is not affected by impregnation of tungsten oxides. The tungsten in the WO₃/TS-1 material existed in the tetrahedral coordination. It was found that the surface silanol groups of TS-1 have interacted with the tungsten oxides. However, tungsten oxide exists in a bulk WO₃ at high amount of tungsten loading. Therefore, it was suggested the formation of Si-O-W bond in the WO₃/TS-1 catalysts.

V. ACKNOWLEDGMENT

We gratefully acknowledge funding from The Ministry of Science Technology and Innovation Malaysia (MOSTI), under IRPA grant no. 09-02-06-0057 SR0005/09-03.

VI. REFERENCES

- [1] Taramasso, M., Perego, G. and Notari, B., U. S. Patents No. 4,410,501. 1983.
- [2] Hollstein, E. J., Wei, J. T. and Hsu, C. Y., U. S. Patent 4,918,041. 1990.
- [3] Clerici, M. G. and Ingallina, P., US Patent No. 5,221,795. 1993.
- [4] Bonino, F., Damin, A., Ricchiardi, G., Ricci, M., Spano, G., D'Aloisio, R., Zecchina, A., Lamberti, C., Prestipino, C. and Bordiga, S., *J. Phys. Chem. B.* 108(11): 3573-3583. 2004.
- [5] Prasetyoko, Z., Ramli, S. Endud and H. Nur, *J. Mol. Catal. A. Chemical* 241. 118. 2005.
- [6] Santiesteban, J. R., Vartuli, J. C., Han, S., Bastian, R. D. and Chang, C. D., *J. Catal.* 168: 431-441. 1997.
- [7] Sohn, J. R. and Park, M. Y., *Langmuir* 14: 6140-6145. 1998.
- [8] Onfroy, T., Clet, G. and Houalla, M., *J. Phys. Chem. B.* in press. 2005.
- [9] Gutiérrez-Alejandre, A., Castillo, P., Ramírez, J., Ramis, G. and Busca, G., "Appl. Catal." A: *General* 216: 181-194. 2001.
- [10] Wang, Y. Chen, Q. Yang, W. Xie, Z. Xu, W. and Huang, D., "Appl. Catal." A: *General* 250(1): 25-37. 2003.
- [11] Xu, B., Dong, L., Fan, Y. and Chen, Y. (2000). *J. Catal.* 193(1) 88-95. 2000.
- [12] Lucas, A., Valverde, J. L., Cañizares, P. and Rodriguez, L., "Appl. Catal." A: *General* 172(1): 165-176. 1998
- [13] Benitez, V. M. and Fígoli, N. S., *Catal. Commun.* 3(10): 487-492. 2002
- [14] Benitez, V. M., Querini, C. A. and Fígoli, N. S., "Appl. Catal." A: *General* 252(2): 427-436. 2003.
- [15] Yori, J. C., Vera, C. R. and Parera, J. M. (1997). "Appl. Catal." A: *General* 163(1-2): 165-175. 1997.
- [16] Logie, V., Maire, G., Michel, D. and Vignes, J. -L., *J. Catal.* 188(1): 90-101. 1999.
- [17] Lau, C., Brück, S., Mai, H. -J. and Kynast, U., *Microporous and Mesoporous Mater.* 47: 339-344. 2001.
- [18] Ramírez, J. and Alejandre, A. G., *J. Catal.* 170(1): 108-122. 1997.
- [19] Astorino, E., Peri, J. B., Willey, R. J. and Busca, G., *J. Catal.* 157: 482-500. 1995.
- [20] Zecchina, A., Bordiga, S., Spoto, G., Marchese, L., Petrini, G., Leofanti, G. Padovan, M., *J. Phys. Chem.* 96(12): 4991-4997. 1992.